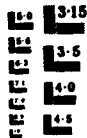
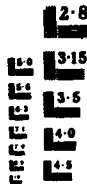


EFFECTS OF TURBULENCE ON STATIONARY AND NON-STATIONARY PROCESSES IN C-SYS (U) ILLINOIS UNIV AT URBANA DEPT OF AERONAUTICAL AND ASTRONAUTICA T A ROBERTS ET AL 1/1
JUN-03-005-03 4-05068-TR-07-0000 546 24 1/2 NI

01 JUN 87 AAE-87-1 AFOSR-TR-87-0980

F/G 21/2

ML



AD-A186 215

AFOSR-TR. 87-0980

2


AAE 

AERONAUTICAL AND ASTRONAUTICAL ENGINEERING DEPARTMENT

~~EFFECTS OF TURBULENCE ON STATIONARY AND NON-STATIONARY~~
Processes in C-Systems

Prepared by

Ted A. Roberts⁽¹⁾ and Robert A. Beddini⁽²⁾
Aerothermal Simulations Laboratory
Department of Aeronautical and Astronautical Engineering
University of Illinois at Urbana-Champaign
104 S. Mathews Avenue
Urbana, Illinois 61801-2997

DTIC
ELECTE
OCT 01 1987
S  D
O&D

DTIC FILE COPY

ENGINEERING EXPERIMENT STATION, COLLEGE OF ENGINEERING, UNIVERSITY OF ILLINOIS, URBANA

DISTRIBUTION STATEMENT A

Approved for public release;
Distribution Unlimited

87 9 24 19

2

FINAL TECHNICAL REPORT
NO. AAE 87-1 UILU ENG 870501

for the period
1 September 1985 through 30 November 1986
for research supported under grant AFOSR-85-0348
Air Force Office of Scientific Research
Dr. Julian M. Tishkoff/NA, Program Manager
Bolling AFB, DC 20332-6448

Effects of Turbulence on Stationary and Non-Stationary
Processes in C-Systems

Prepared by

Ted A. Roberts⁽¹⁾ and Robert A. Beddini⁽²⁾
Aerothermal Simulations Laboratory
Department of Aeronautical and Astronautical Engineering
University of Illinois at Urbana-Champaign
104 S. Mathews Avenue
Urbana, Illinois 61801-2997

DTIC
ELECTE
S OCT 01 1987 D
D

DISTRIBUTION STATEMENT

Approved for public release
Distribution Unlimited

- (1) Graduate Research Assistant
(2) Associate Professor and Principal Investigator

Unclassified

SECURITY CLASSIFICATION OF THIS PAGE

ADA186215

REPORT DOCUMENTATION PAGE

Form Approved
OMB No. 0704-0188

1a. REPORT SECURITY CLASSIFICATION Unclassified			1b. RESTRICTIVE MARKINGS	
2a. SECURITY CLASSIFICATION AUTHORITY			3. DISTRIBUTION / AVAILABILITY OF REPORT Approved for public release; distribution is unlimited.	
2b. DECLASSIFICATION / DOWNGRADING SCHEDULE				
4. PERFORMING ORGANIZATION REPORT NUMBER(S) AAE 87-1 UILU ENG 870501			5. MONITORING ORGANIZATION REPORT NUMBER(S) AFOSR-TR-87-0980	
6a. NAME OF PERFORMING ORGANIZATION Board of Trustees University of Illinois		6b. OFFICE SYMBOL (if applicable)	7a. NAME OF MONITORING ORGANIZATION AFOSR/NA	
6c. ADDRESS (City, State, and ZIP Code) 506 S. Wright Street Champaign, Illinois 61820		7b. ADDRESS (City, State, and ZIP Code) Building 410, Bolling AFB DC 20332-6448		
8a. NAME OF FUNDING / SPONSORING ORGANIZATION AFOSR/NA		8b. OFFICE SYMBOL (if applicable) NA	9. PROCUREMENT INSTRUMENT IDENTIFICATION NUMBER AFOSR 85-0348	
8c. ADDRESS (City, State, and ZIP Code) Building 410, Bolling AFB DC 20332-6448		10. SOURCE OF FUNDING NUMBERS		
		PROGRAM ELEMENT NO. 61102F	PROJECT NO. 2308	TASK NO. A1
11. TITLE (Include Security Classification) (U) Effects of Turbulence on Stationary and Nonstationary Processes in C-Systems				
12. PERSONAL AUTHOR(S) Ted A. Roberts and Robert A. Beddini				
13a. TYPE OF REPORT Final Technical		13b. TIME COVERED FROM 9-1-85 to 11-30-86	14. DATE OF REPORT (Year, Month, Day) 87-June - 01	15. PAGE COUNT 34
16. SUPPLEMENTARY NOTATION (continued)				
17. COSATI CODES			18. SUBJECT TERMS (Continue on reverse if necessary and identify by block number)	
FIELD	GROUP	SUB-GROUP		
2102	2108	2001	ACOUSTIC INSTABILITY; AEROACOUSTICS; SOLID PROPELLANT ROCKET ENGINES; TRANSPIRATION; TURBULENT BOUNDARY LAYER; ACOUSTIC BOUNDARY LAYER; COMBUSTION INSTABILITY; (OVER)	
19. ABSTRACT (Continue on reverse if necessary and identify by block number) Turbularization of an acoustic boundary-layer (Stokes layer) on impermeable and permeable surfaces is analytically considered. The theoretical approach utilizes a second-order closure model of turbulence. Both an approximate, closed-form solution and a more comprehensive finite difference solution of the time dependent, parabolic, one-dimensional governing equations are obtained. For simple acoustic boundary-layers on impermeable surfaces, both the approximate solution and the numerical results for the critical acoustic Mach number required for turbulent transition are qualitatively confirmed by experiment. The calculations for acoustic boundary-layers with transpiration (injection) indicate a substantial reduction of the acoustic Mach number required for transition, up to a limiting injection velocity that is frequency dependent. The results may provide a mechanism for flow-related combustion instability in practical (Over)				
20. DISTRIBUTION / AVAILABILITY OF ABSTRACT <input checked="" type="checkbox"/> UNCLASSIFIED/UNLIMITED <input checked="" type="checkbox"/> SAME AS RPT <input type="checkbox"/> DTIC USERS			21. ABSTRACT SECURITY CLASSIFICATION Unclassified	
22a. NAME OF RESPONSIBLE INDIVIDUAL Julian M Tishkoff			22b. TELEPHONE (Include Area Code) (202) 767-4935	22c. OFFICE SYMBOL AFOSR/NA

Abstract

Turbularization of an acoustic boundary-layer (Stokes layer) on impermeable and permeable surfaces is analytically considered. The theoretical approach ^{uses} ~~utilizes~~ a second-order closure model of turbulence. Both an approximate, closed-form solution and a more comprehensive finite difference solution of the time dependent, parabolic, one-dimensional governing equations are obtained. For simple acoustic boundary-layers on impermeable surfaces, both the approximate solution and the numerical results for the critical acoustic Mach number required for turbulent transition are qualitatively confirmed by experiment. ~~The~~ calculations for acoustic boundary-layers with transpiration (injection) indicate a substantial reduction of the acoustic Mach number required for transition, up to a limiting injection velocity that is frequency dependent. The results may provide a mechanism for flow-related combustion instability in practical systems, particularly solid propellant rockets, since turbularization of the near-surface combustion zone could result at relatively low acoustic Mach numbers.

This final report documents a completed phase of work performed under the subject grant, the scope of which ^{is concerned with} ~~concerns~~ the analysis of turbulent flow and heat transfer behavior in rocket chamber flows (C-systems). Further work is ongoing under a new grant number.



Accession For	
NTIS CRA&I	<input checked="checked" type="checkbox"/>
DTIC TAB	<input type="checkbox"/>
Unannounced	<input type="checkbox"/>
Justification	
By	
Distribution/	
Availability Codes	
Dist	Avail and/or Spec
A-1	

Foreword

This report documents a completed initial phase of work performed under grant AFOSR 85-0348, the subject of which concerns the analysis of turbulent flow and heat transfer behavior in rocket chamber flows (presently termed C-systems). The overall scope of work includes the analysis of turbulence development and behavior in chemical and advanced thermal propulsion systems. Specific topics addressed include combustion instability in solid propulsion systems and methods of heat transfer reduction in advanced thermal propulsion systems.

The initial approach to these problems involves assessment of their parametric dependence utilizing a well characterized second-order turbulence closure model. Subsequently, large-eddy simulation methods will be developed for these highly energetic and transitional flows.

This work is continuing under a new grant (AFOSR 86-0319).

Table of Contents

Abstract	1
Foreword	11
1. Introduction	1
2. Analysis	4
3. Results and Discussion	13
4. Conclusions	17
5. Acknowledgment	18
6. References	19
7. Nomenclature	22
8. Publications	24
9. Personnel	24
10. Technical Interactions	25
11. Figures	26

1. Introduction

Oscillatory flows in ducts can be sustained by a variety of interactions. These range from purely fluid-dynamically induced motions (e.g., large scale vortex shedding or shockwave instability), to the more energetic motions possible with diabatic flows. Particularly severe oscillations can occur in solid propellant rocket chambers, for example, wherein the oscillatory motion can be driven by interactions with the substantial energy release inherent in near-surface combustion processes.

Prior analytical work in "combustion" instability in solid rockets has identified some of the mechanisms which can produce velocity-field coupling to the overall instability process (see, for example, the review by Culick¹). These studies have shown that for a simple longitudinal standing acoustic wave in a duct, a Rayleigh diabatic instability criterion can result which is dependent upon the oscillatory motion of the gas column. Since the energy release occurs in the near surface region, analytical work has addressed acoustic boundary-layer effects on propellant combustion response (see, for example, Lengele²). Implicit in several response function analyses is the assumption that the acoustic boundary-layers behave quasi-steadily and in phase with the longitudinal acoustic velocity outside the boundary layer.

Recent work on combustion-flowfield interactions in solid rocket chambers has analytically and experimentally examined fundamental fluid-dynamic aspects of mean flow, acoustic wave and turbulence behavior. Hydrodynamically modeling the flow with a semi-enclosed, porous-walled duct (with large injection through the wall), Brown et al^{3,4} experimentally confirmed the transitional behavior of the mean flow predicted in Reference 5. The major emphasis of this non-reactive flow experiment was to investigate the effect of low and moderate amplitude forced acoustic oscillations on the flow, using both hot-wire anemometry and surface-mounted hot-film sensors.

Basing their conclusions on the surface sensor measurements, Brown, et al suggested that near surface turbulence produced by the mean-flow transition process appeared to "destroy" the coherent response of the sensors downstream of transition. Consequently, for low acoustic amplitudes, a surface response capable of inducing instability would most probably originate in the head end (pre-transition) section of a rocket chamber. However, it is noted that for large axial distances, low amplitude acoustic signals appear to be resurrected in the post transition region. Lower amplitude harmonics of the driving frequency were observed by Brown in both the surface and hot wire measurements. Their existence is consistent with the nonlinear behavior of a (potentially thick) acoustic boundary layer (Stokes layer).

Analyses of laminar acoustic boundary-layer phenomena involved in propellant response have been offered by Flandro⁶; Glick and Renie⁷; Ben Reuven⁸ and Hedge, et al⁹. Baum and Levine¹⁰ utilized a full unsteady Navier-Stokes solution method; their results showed a Stokes layer persisting even in the presence of strong injection velocities. The thickness of the Stokes layer was of the same order as the Stokes layer for noninjected flow. The presence of vortices above the acoustic boundary layer were also indicated in the results. Although several aspects of these analyses are interesting, the following important point is noted. Simple scaling estimates of the laminar acoustic boundary layer height (the Stokesian thickness) $\delta_a = \sqrt{\nu/f}$ indicate that δ_a is well above the gas-phase flame height except for very high frequencies ($f \gtrsim 10^4$ Hz). Consequently, minimal acoustic velocity interaction with combustion would be expected at low to intermediate frequencies as indicated, for example, by the more detailed analysis of Reference 6. Although this does not preclude "velocity coupled" instability resulting from laminar interactions (whether linear or nonlinear), it does suggest that other mechanisms of interaction should be explored.

Toward this end, the potential for the laminar acoustic boundary-layer to undergo transition to turbulence is considered. It is well established that for piston driven closed duct flows (viz., in which there is negligible mean axial flow), longitudinal acoustic waves of a few percent relative pressure amplitude can induce turbulence within the Stokes layer. The literature review and independent data of Merkli and Thomann¹¹, for example, confirm a critical amplitude which varies as \sqrt{f} for this type of simple acoustic motion. Thus, for fixed amplitude, lower frequency disturbances are more likely to produce turbulence.

It is known from studies of quasi-steady propellant/flowfield interactions that even small levels of turbulence within the combustion zone can appreciably enhance propellant combustion rates. Whether acoustically induced turbularization can occur in actual rocket chambers depends upon several complex effects including the presence of large injection rates, surface roughness, and of course, the specific type of combustion process. In one experiment¹², values of the threshold velocity for propellant response ("acoustic erosivity") were lowered by a factor of 2 relative to steady state conditions.

The objective of the present analysis is to consider, under several simplifying assumptions, the general trends of acoustic boundary-layer turbularization on a permeable surface in the presence of large injection rates. Though pertinent to the issues discussed previously, the posed problem is more fundamental and of potentially broader interest.

2. Analysis

The motion of a perfect gas described by the Navier-Stokes equations is considered. An arbitrary dependent variable, $g(x_1, t)$ is decomposed according to the notation

$$g(x_1, t) = \bar{g}(x_1, t) + g'(x_1, t)$$

with

$$\bar{g} = \langle g(x_1, t) \rangle + g''(x_1, t) .$$

In these equations, g' is the turbulent fluctuation, \bar{g} is the ensemble average, g'' is the acoustic (deterministic) component and $\langle g \rangle$ is the long-time mean. The remainder of this section is divided into two parts, the first considering order-of-magnitude analysis of the problem and derivation of an approximate relation for critical amplitude of transition from the turbulence model equations. The second part discusses the equations and method used for a more comprehensive numerical solution of the acoustic boundary-layer in the presence of transpiration.

2.1 Order of Magnitude Analysis

Neglecting third order correlations and the axial derivatives of molecular and turbulent stresses, the $\langle \rangle$ average of the axial momentum equation is

$$\begin{aligned} & \frac{\partial}{\partial x} (\langle \rho \rangle \langle u \rangle \langle u \rangle + \langle \rho \rangle \langle u'' u'' \rangle + \langle u \rangle \langle \rho'' u'' \rangle + \langle u \rangle \langle \rho'' u'' \rangle) \\ & + \frac{\partial}{\partial y} (\langle \rho \rangle \langle u \rangle \langle v \rangle + \langle \rho \rangle \langle u'' v'' \rangle + \langle u \rangle \langle \rho'' v'' \rangle + \langle v \rangle \langle \rho'' u'' \rangle) \\ & = - \frac{\partial \langle p \rangle}{\partial x} + \frac{\partial}{\partial y} (\langle \mu \rangle \frac{\partial \langle u \rangle}{\partial y}) + \frac{\partial \langle \tau \rangle}{\partial y} \end{aligned} \quad (1)$$

where the mean turbulent shear stress is $\langle \tau \rangle = -\langle \rho \rangle \langle u' v' \rangle$ (neglecting turbulent density correlations). The equation for the acoustic component (u'') is, to first order:

$$\langle \rho \rangle \frac{\partial u''}{\partial t} + (\langle \rho \rangle u'' + \langle u \rangle \rho'') \frac{\partial \langle u \rangle}{\partial x} + u'' \frac{\partial}{\partial x} (\langle \rho \rangle \langle u \rangle)$$

(1)

(2)

(3)

$$+ \langle \rho \rangle \langle u \rangle \frac{\partial u''}{\partial x} + (\langle \rho \rangle v'' + \langle v \rangle \rho'') \frac{\partial \langle u \rangle}{\partial y}$$

(4)

(5)

$$+ u'' \frac{\partial}{\partial y} (\langle \rho \rangle \langle v \rangle) + \langle \rho \rangle \langle v \rangle \frac{\partial u''}{\partial y} = \frac{-\partial p''}{\partial x}$$

(6)

(7)

(8)

$$+ \frac{\partial}{\partial y} (\langle \mu \rangle \frac{\partial u''}{\partial y}) + \frac{\partial \tau''}{\partial y} \tag{2}$$

(9)

(10)

where $\tau'' = -\langle \rho \rangle \overline{u'v'}$.

In equation (1), the second-order correlations arising from the unsteady motion can produce virtual stresses and convective fluxes analogous to those produced by the turbulent motion alone. These correlations induce the classical phenomenon of "acoustic streaming,"¹⁴ wherein a component of the mean flow is driven by acoustic motion. Of potentially more importance to propellant combustion are the analogous second-order terms which appear in the equation for the transport of thermal energy in the propellant flame zone. While these thermal transport effects will not be analyzed in this study, examples of their importance to effective steady-state heat transfer may be

found in the literature (see, for example, Ref. 13). The effects of steady-state enhancements to heat transfer from acoustic streaming effects have not been considered with respect to the reactive environment in rocket engines, although it is possible that these effects could also produce a coupling mechanism for instability.

The remainder of this analysis will be concerned with equation (2) and the relative importance of various terms within the acoustic boundary layer. To further simplify this equation, it will be assumed that the density in the region of interest is approximately constant and that the v'' produced by propellant response is negligible. These assumptions would necessarily be removed in considering a comprehensive propellant velocity response analysis.

The magnitudes of the terms in Equation (2) are estimated by normalizing the velocities to a_0 , the chamber length to L , chamber radius, to δ , and utilizing the continuity equation and the assumption of a standing first longitudinal acoustic mode. It is also assumed that the turbulence shear stress may be scaled by $\tau'' = c_\tau \langle \rho \rangle u''^2$, where $|c_\tau| \ll 1$. The respective orders of the terms in Equation (2) are then

$$\{1, \langle M \rangle, \langle M \rangle, \langle M \rangle, (\delta_a / \delta) \langle M \rangle, \langle M \rangle, (a / f \delta_a) \langle M_s \rangle, 1, v / f \delta^2 a, c_\tau a / (f \delta_{a,turb}) M''\}.$$

The order unity terms 1 and 8 recover the inviscid acoustic mode solution in the central region of the duct. A considerable simplification results if $\langle M \rangle$ is small, since terms 2 through 6 may be dropped without fundamentally altering boundary layer characteristics retained in terms 7,9,10. (It is important to note that the maximum response to the surface sensors in Reference 4 occurs in the head end region, where $\langle M \rangle$ is $\lesssim 0.1$.) Neglecting for the moment the transverse convection and turbulence terms, it is seen that for the viscous term to be of order unity implies the Stokes estimate,

$$\delta_a \sim \left(\frac{u}{F}\right)^{1/2} \quad (3)$$

and is the smallest possible laminar boundary-layer height of the problem. The effects of injection on the acoustic boundary layer (provided largely by term 7) can be substantial and even dominate. The ratio between the convection and viscous terms in Equation (3) is of the order 10 under conditions of interest.

The additional shear stress provided by term 10 in Equation (2), as well as the analogous additional heat flux appearing in the energy equation, result from possible turbulent motions. Further, it is noted that term 10 is the only term which depends on the amplitude of the acoustic motion. (The acoustic amplitude, M'' , is a linear scaling parameter of all other terms but occurs quadratically in the turbulent shear term), thus posing the question of a possible relation to nonlinear stability phenomena.

As noted in reference¹¹, there are a few approaches which can be employed to obtain a stability or transition criterion for the acoustic boundary layer. In the approach adopted here, the second-order modeling equations employed in reference³ are considered (see also section 2.2). Preliminary operations and assumptions are summarized as follows. Equations for the velocity correlations $\overline{u'_i u'_j}$ are contracted to obtain an equation for the turbulence intensity $q^2 = \overline{u'_i u'_i}$. Fluid material properties are assumed constant, and the turbulence (or preturbulent disturbance level) is assumed small so that third and higher order velocity correlations may be neglected. It is also assumed as an approximation that $\overline{u' u'} = a_{uu} q^2$, $\overline{v' v'} = a_{vv} q^2$, and $\overline{u' v'} = a_{uv} q^2$, where a_{uu} , a_{vv} and a_{uv} are constants. Substituting these relations into the q^2 equation, taking the mean flow to be negligible, and applying boundary layer assumptions for a quasi-planar condition yields:

planar condition yields:

$$\begin{aligned} \rho \left(\frac{\partial q^2}{\partial t} + u'' \frac{\partial q^2}{\partial x} + v'' \frac{\partial q^2}{\partial y} \right) + 2\rho q^2 \left(a_{uu} \frac{\partial u''}{\partial y} + a_{uv} \frac{\partial u''}{\partial y} \right) \\ = -2A \frac{\mu q^2}{\Lambda^2} + \frac{\mu \partial^2 q}{\partial y^2} \end{aligned} \quad (4)$$

where Λ is the disturbance macrolength - scale and A is a constant used in modeling low turbulent Reynolds number dissipation. The approximation $\Lambda = C_\Lambda \delta_a$ (where δ_a is specified by Equation (3)), is also employed to evaluate the maximal effective length scale appropriate for the acoustic boundary layer.

Equation (4), which is linear in q^2 , may be order-of-magnitude scaled in the same manner as Equation (2). The requirement that $\frac{\rho D q^2}{Dt} = 0$ (for neutral stability) may be imposed if the Reynolds number $u'' \delta_a / \nu \lesssim O(1)$. The order of magnitude analysis indicates that the fifth (production) term on the left hand side and the first (dissipation) term on the right hand side of equation 2 are dominant, resulting in the stability criterion

$$M_{cr}'' = \frac{A}{(-a_{uv}) C_\Lambda^2} \frac{(fu)^{1/2}}{a_o} = K \frac{(fv)^{1/2}}{a_o}. \quad (5)$$

Utilizing the turbulence modeling constants specified in the Appendix of Reference (3) (i.e., $A = 3.25$, $C_\Lambda = .17$), and estimating $a_{uv} = -.15$ from fully developed flat-plate turbulent boundary layer flows, yields an estimate of $K = 750$. Merkli and Thomann cite prior experimental values of K ranging from 188 to 915, and obtained the value $K = 501$ in their own experiments. (The constant K in Equation (5) is related to the Merkli and Thomann constant A_c

by $K = A_c \sqrt{(2\pi)/2}$. They speculated that the variation in K observed in prior studies could be caused by variations in the roughness of the duct surface, and demonstrated that disturbances caused by the anemometer probe can also appreciably affect K .

The critical Mach number given by Equation (5) is shown in Figure 1 together with the data of Merkli and Thomann. As can be seen, the functional dependence is correct, and even the very approximate estimates of physical constants and empirical parameters yield quantitative agreement to within several percent of the data. To the authors' knowledge, the derivation of an approximate transition relation from linearizing this type of complex turbulence model is novel.

2.2 Computational Analysis

The second-order turbulence closure approach developed by Donaldson and colleagues^{16,17} was implemented in Reference 3 as a parabolized model for calculating statistically stationary, compressible transitional flows in porous walled ducts with large injection rates. The assumptions and order-of-magnitude analysis of the previous section again yield a parabolic equation system for the present acoustic boundary-layer problem. Computationally, the axial convection terms $\bar{\rho} u \partial g / \partial x$ (where g is an arbitrary dependent variable) are replaced by $\bar{\rho} \partial g / \partial t$ for the present case. With the exception of $\partial \bar{p} / \partial x$ in the momentum equation, all other axial derivatives are taken to be null. The continuity equation,

$$\frac{\partial \bar{\rho}}{\partial t} + \frac{1}{r} \frac{\partial}{\partial r} [r^v (\bar{\rho} v + \bar{\rho}' v')] = 0$$

and the $\partial \bar{p} / \partial t$ term on the right hand side of the energy equation are retained, however, for planned work involving energetic flows.

The parabolic differential equation system may be considered in the functional form

$$\begin{aligned} & \bar{\rho} \frac{\partial g}{\partial t} + \bar{\rho} \bar{v} \frac{\partial g}{\partial r} \\ & = \frac{1}{r} \frac{\partial}{\partial r} (r^v \bar{\mu}_g \frac{\partial g}{\partial r}) + G_g(f) \end{aligned} \quad (6)$$

where $g = \{\bar{u}, \bar{h}, \overline{u'u'}, \overline{v'v'}, \overline{w'w'}, \overline{u'v'}, \overline{h'u'}, \overline{h'v'}, \overline{h'h'}\}^T$, u , v and w are the axial, radial and circumferential velocity components, v is here the index for planar or axisymmetric geometry, ρ the density and $h = c_p T$ is the specific static enthalpy. The molecular transport coefficient μ represents the dynamic viscosity (μ) or the thermal conductivity parameter, $\sigma = k/c_p$, as appropriate for each equation. However, not all of the molecular diffusion terms for each equation in the system may be cast in the form shown in Equation (2). Those that do not conform are implicitly contained within the complex functions G_g , which also represent the sources, cross-coupling and dissipation terms for the equations. Although the more general ($\bar{}$) averaging is used in the above notation, the only mean velocity component retained is \bar{v} , which is nearly equal to $\langle v \rangle$ in this study because of the approximately isothermal and isobaric conditions assumed.

The pressure along the duct, $\bar{p} = \langle p \rangle + p''(x, t)$, is specified by the one-dimensional standing wave solution

$$p'' = \Pi_{ma} \langle p \rangle \cos(n\pi x/L) \cos(n\pi f t) \quad (7)$$

where Π_{ma} is the maximum relative acoustic pressure amplitude, and $u_{ma} = \Pi_{ma} a_0 / \gamma$. All calculations to be presented were performed at the velocity antinode of the first longitudinal mode. Material properties were those of air at standard conditions.

The turbulence length scale, Λ , in this model is algebraic and described³ by a linear variation from its surface value, Λ_s ($\Lambda_s = 0$ for smooth walls), to a plateau level proportionate (with constant, C_Λ) to the thickness of the shear flow. For the present analysis this thickness was defined as δ_{aa} , equal to the height above the surface where the boundary asymptotes to 99% of u''_c . For injected flows, however, waves are convected away from the surface. In these cases the first zero-crossing of u'' was taken as the effective δ_{aa} . The final values of δ_{aa} used in the length scale expression were smoothed by integrating in time. An alternative differential length-scale equation is desirable, but much has been written concerning problems with the low turbulent Reynolds number behavior of such equations.

Boundary conditions at the duct centerline (or centerplane) are the symmetry conditions, which for the posed system are

$$\begin{aligned} \frac{\partial}{\partial r} [\bar{u}, \bar{h}, \overline{u'u'}, \overline{v'v'}, \overline{w'w'}, \overline{h'h'}, \overline{h'u'}] &= 0 \\ &= \overline{u'v'} = \overline{h'v'} \quad . \end{aligned}$$

Due to the final form of the governing equations, the requirement that $\bar{v} = 0$ on the centerline (centerplane) is necessarily relaxed. At the duct surface, the static enthalpy corresponding to a given temperature is specified, and the mean injection velocity, \bar{v}_s , is prescribed. The no-slip condition implies that all tangential velocity components and their correlations are zero. Experiments have confirmed that strong injection rates through a porous plate can produce pseudo-turbulent disturbances which must be included in the ensemble average of the $\overline{v'v'}$ boundary condition. The parameter $\sigma_v^2 = \overline{v'v'}/\bar{v}^2$ was introduced in Ref. 3 to account for this important source of disturbance. All enthalpy correlations are null due to

the prescribed uniform surface enthalpy.

The initial profile for the axial velocity component was taken to be the analytical solution (at $t = 0$) of Sexl and Uchida (in Schlichting¹⁸) for oscillatory flow in a cylindrical duct. Initial profiles of the normal Reynolds stresses were taken to be isotropic, and proportionate to the square of the initial velocity profile. The peak initial disturbance level, $q_{\max}(t = 0, y)/u_{ma}$, was assumed to be 0.01 for all calculations reported here.

The implicit numerical procedure and adaptive grid are described in prior studies. Except where noted, approximately 50 time steps per period were employed. The number of spatial nodes within the boundary layer varied from about 40 for laminar flows to about 75 for turbulent cases.

3. Results and Discussion

Normalized profiles of the axial velocity in the laminar acoustic boundary layer ($f = 1000$ Hz, $\delta_a = 180$ μ m) are shown for various times within a period in Figure 2. The results display the classical phase shift and Richardson annular effects due to viscosity. These calculations were performed with 100 time steps per period and produce a relatively small computational error, principally outside the boundary layer and near the maxima in the acoustic velocity. Since a large number of calculations were needed for the transition studies, the number of time steps per period was halved for those calculations, and the error in the calculated acoustic velocity was then approximately doubled.

Figure 3 shows the profiles for a fully (cyclically) turbulent boundary layer at 100 Hz with $\Pi_{ma} = .125$. There is a noticeable diffusion of the Richardson effect and a pronounced increase in the velocity gradient near the surface. However, a protracted law-of-the-wall (logarithmic) region is not observed.

Figure 4 shows normalized turbulence intensity profiles, q/u_{ma} , in the boundary layer for the same conditions stated for Figure 3. The calculated peaks in turbulence level are comparable to those calculated for steady state flows ($\approx 15\%$). To within computational accuracy, these peaks are symmetric with respect to $\pm\pi ft$. A slight phase lag, on the order of 5-10 degrees, exists between the intensity maxima and the rectified acoustic velocity $|u''_c|$. This lag increases at higher frequencies. Also note that the intensity decreases substantially, but is not predicted to vanish at the zero-crossings of u''_c .

Figure 5 shows turbulent velocity profiles for a Stokes layer with injection at $f = 100$ Hz, $\Pi = 0.080$, $\langle v \rangle = 1$ m/s. A pronounced Richardson

effect is evident, surpassing even the laminar noninjected results. The estimated value of the effective boundary layer thickness for this case was 5.5 mm (approximately $y/\delta_a = 14$ in the Figure). The convective wave-train behavior shown was also evident in the laminar injected Stokes layer calculations of Reference 7.

Figure 6 shows the corresponding normalized turbulence intensity profiles. Due, in part, to the enhanced Richardson effect, very large intensity levels ($\approx 30\%$) are predicted. As turbulence is produced in the inner layer at a later time in the cycle, the velocity wave formed from an earlier cycle produces a harmonic wave in the intensity profile ($ft = 5.125$). A long tail is predicted due to large decay times and the fact that turbulence is beginning to accumulate at the computational centerline ($\delta = 5$ cm) where the symmetry condition is employed. In an actual duct flow environment, the mean axial flow would convect these tails downstream as they interact with mean flow induced turbulence.

Calculated results for the critical acoustic Mach number at transition, $M''_{cr} = \Pi_{cr}/\gamma$, are shown in Figure 1 together with the approximate relation and data for non-injected Stokes layers. The functional dependence is similar, but the proximity of the calculations to the $K = 750$ line is coincidental. Note, for example, that although not shown here, the numerical results display a dependence on the initial amplitude of turbulence assumed. "Transition" in the calculated results was determined by monitoring the growth or decay of initial turbulence from the initial value over several cycles. For the cases with injection, the growth rates were not as strongly dependent on Π as were those for the non-injected cases.

Critical Mach numbers for transition as a function of the normalized mean injection velocity, $\langle v \rangle / (fv)^{1/2}$, are shown in Figure 7 for three frequencies,

$f = 100, 300$ and 1000 Hz. A pronounced decrease in M''_{cr} is predicted with increasing injection velocity such that all curves exhibit a minimum that is frequency dependent. The minima are almost a factor of three below the M''_{cr} for noninjected Stokes layers. As an example, the 100 Hz non-injected Stokes layer is calculated to have $M''_{cr} = .083$. The minimum value of $M''_{cr} = .025$ occurs at $\langle v \rangle = 0.25$ m/s, while $M''_{cr} = .048$ at $\langle v \rangle = 1.0$ m/s (the termination of the line at this frequency).

Even more informative are the same results for transition normalized not as a critical acoustic Mach number, but as a critical acoustic Reynolds number, $u_{ma}/(fv)^{1/2}$. In this case, all three curves for frequency in Figure 7 collapse onto a single line (to within computational precision), shown as the upper line in Figure 8. This figure also shows results for finite levels of the surface disturbance parameter, $\sigma_v = 0.035$ and 0.07 for two different transition criteria to be discussed. The accompanying value of Λ_s assumed in the calculations was 3×10^{-4} m. These values are viewed as realistic and perhaps conservative. It is not surprising that this finite disturbance effect, which continuously "feeds" the injected layer, is predicted to yield further reduction in critical acoustic Reynolds number, analogously to quasi-steady flows.³ As a specific example, the minimum critical Mach number for the 100 Hz case at $\langle v \rangle = .20$ m/s is decreased to approximately one percent for $\sigma_v = .035$.

As mentioned earlier, it was more difficult to determine the value of r for cases with injection and finite levels of σ_v present. The first criterion employed consisted of monitoring the maximum turbulence level, q_{max}/u_{ma} , occurring at any height within the boundary layer. If this maximum attained a value of 0.07 or greater within 3 cycles, the flow was considered turbulent. Using this criterion, the $\sigma_v = 0$ lines were computed along with

the alternating-dashed lines for $\sigma_v = 0.035$ and 0.07 . While this criterion was satisfactory for $\sigma_v = 0$ cases, it proved to be unsatisfactory for cases with finite levels of σ_v .

To illustrate this effect, Figures 9a, b., and c show the variation of turbulence intensity versus normalized time at $y = \delta_a$, for three values of Π , $\langle v \rangle = 0.25$ m/s and $\sigma_v = 0$. It is evident from curves 9a and b that a very small increase in Π is able to cause the flow to transition to a cyclically turbulent condition.

When finite levels of σ_v are included the determination of Π_{cr} becomes more complicated. Figures 10a, b, and c are results for $\langle v \rangle = 0.25$ m/s and $\sigma_v = 0.035$. Figure 10a is a case for which the turbulence bursts to a q/U_{ma} level of approximately 0.24 but then dissipates over 10 cycles until only the low level turbulence due to σ_v is still present. Figures 10b and c illustrate the increase in Π required to achieve the cyclic behavior which we considered to be characteristic of a turbulent case. This criterion for transition was used to calculate the dashed curves for $\sigma_v = 0.035$ and 0.07 in Figure 8.

To recapitulate the results of the two transition criteria, the alternating dashed lines in Figure 8 qualitatively represent a "burst" or transient criterion for transition, while the dashed lines represent the particular (long-time) criterion. For the latter case, regions to the right of the nearly vertical line segments are indicated to be turbulent. The difference between the two criteria is in part explained by Equation (4), which must be augmented by the term $\bar{\rho} \langle v \rangle \frac{\partial q^2}{\partial y}$ when σ_v is finite. This can result in three different turbulence time scales being competitive in specific parametric cases

4. Conclusions

An analysis of transitional and turbulent acoustic boundary layers in the presence of strong injection has been presented. The problem was approached by analyzing the behavior of a second-order turbulence model rather than the traditional Orr-Sommerfeld linearization. The approximate, order-of-magnitude analysis provides a simple and functionally correct estimate of transition for simple acoustic boundary-layers. This technique may prove useful for estimating the stability characteristics of other types of flows.

The computed results for Stokes layers with injection indicate a substantial increase in the acoustic boundary layer thickness for strongly injected laminar or turbulent flows, but no "blow-off" condition is observed. For injected fully turbulent flows, a pronounced Richardson effect is obtained and is accompanied by very large maximum levels of turbulence (> 20%). Both axial velocity and turbulence profiles exhibit a convected wave train shape. The turbulence development was also found to lag the rectified acoustic velocity by a few degrees at lower frequencies.

Transition results for conventional Stokes layers are in agreement with the approximate analysis and data trends, although at the higher acoustic amplitudes shown by the scaling relation, additional nonlinear effects would be important. The effect of injection is to (non-monotonically) decrease the critical acoustic Mach number for transition by up to a factor of about three. This effect is frequency dependent, but is expressible in terms of the acoustic and injection Reynolds numbers for the problem.

A further appreciable reduction in critical Mach number (or Reynolds number) is predicted for injection velocities with finite, continuous disturbance levels. This effect is strong enough to indicate that at the

minimum critical acoustic Reynolds number, rather modest levels of acoustic pressure ratio ($\sim 1\%$) can induce significant turbulence levels near the surface.

The potential for turbularization of a near-surface reaction zone in ducted flows such as rocket chambers therefore theoretically exists. However, whether this mechanism can produce instability in such systems depends upon several effects not considered in this investigation. For example, combustion processes and (acoustically) nonlinear behavior such as thermoacoustic streaming could influence the nature of the overall response, while the axial mean flow could bias the transitional characteristics over the acoustic velocity and pressure cycles. Further research on these topics is in progress.

5. Acknowledgment

This research was supported, in part, by the Air Force Office of Scientific Research (AFSC) under grant AFOSR 85-0348. Drs. Leonard Caveny, Robert Vondra, and Julian Tishkoff served as Program Managers.

6. References

- 1) Culick, F. E. C., "Stability of Longitudinal Oscillations with Pressure and Velocity Coupling in a Solid Propellant Rocket", Comb. Sci. and Technology, Vol. 2, No. 2, pp. 179-201.
- 2) Lengele, G., "A Model Describing the Velocity Response of Composition Propellants", AIAA J., Vol. 13, 1975, pp. 315-322.
- 3) Brown et al (1984) "Coupling Between Velocity Oscillations and Solid Propellant Combustion", Journal of Propulsion and Power, Vol. 2, No. 5, Sept. 1986, pp. 428-437.
- 4) Brown, R. S., Blackner, A. M., Willoughby, P. G. and Dunlap, R., "Coupling Between Velocity Oscillations and Solid Propellant Combustion", AIAA Paper No. 86-0531, 24th Aerospace Sciences Mtg., January, 1986.
- 5) Beddini, R. A. "Injection-Induced Flows in Porous Walled Ducts", AIAA J., Vol. 24, No. 12, November, 1986, pp. 1766-1773.
- 6) Flandro, G. A. (1982), "Nonlinear Time-Dependent Combustion of a Solid Rocket Propellant", Proc. 19th JANNAF Combustion Meeting, October 1982, CPIA Pub. 366, Vol. II, pp. 111-122.
- 7) Glick, R. L. and Renie, J. P., "On the Oscillatory Flowfield in Solid Rocket Motors", Proc. 20th JANNAF Combustion Meeting, CPIA Pub., October 1983.

- 8) Ben Reuven, M. "The Viscous Wall-Layer Effect in Injected Porous Pipe Flow," AIAA J., Vol. 24, No. 2, 1986, pp. 284-292.
- 9) Hedge, U. G., Chen, F. L. and Zinn, B. T., "Investigations of Reactive and Non-reactive Acoustic Boundary Layers on Porous Walled Ducts", AIAA Paper No. 85-0235, 23rd Aerospace Sciences Meeting, January, 1985.
- 10) Baum, J. D. and Levine, J. N. (1986), "Numerical Study of Flow Turning Phenomenon", AIAA Paper No. 86-0533, AIAA 24th Aerospace Sciences Meeting, January 1986.
- 11) Merkli, P., and Thomann, H., "Transition to Turbulence in Oscillating Pipe Flow", J. Fluid Mech. 68, Part 3, 1975, pp. 567-575.
- 12) Gostinsev, Yu. A. and Pokhil, P. F., "Relation of Two Combustion Anomalies of Powder Tubes", Dok. Akad. Nauk SSSR, 188, pp. 135-136 (translated in Soviet Physics).
- 13) Keith, H. G., and Purdy, K. R., "Laminar Forced Convection Under the Influence of a Resonant Acoustic Field," Proc. 1967 Heat Transfer and Fluid Mech. Institute, ed: Libby, Olfe, and Van Atta, Stanford University Press, pp. 298-315.
- 14) Lin, C. C., "Motion in the Boundary Layer with a Rapidly Oscillating External Flow", Proc. 9th Int. Congress Appl. Mech., Brussels, 1957, vol. 4, pp. 155-167.

- 15) Lin, C. C., Theory of Hydrodynamic Stability, Cambridge University Press, 1955, Chapter 3.
- 16) Donaldson, C. duP., "Calculations of Turbulent Shear Flows for Atmospheric and Vortex Motions", AIAA J. 10, 1, (1972), pp. 4-12.
- 17) Varma, A. K., Beddini, R. A., Sullivan, R. D. and Donaldson, C. duP., "Application of an Invariant Second-Order-Closure Model to the Calculation of Compressible Boundary Layers", AIAA Paper No. 74-592, AIAA 7th Fluid and Plasma Dynamics Conference, June, 1974.
- 18) Schlichting, H., Boundary Layer Theory, 6th edition, trans. by J. Kestin, McGraw Hill, NY, 1968, p. 421.

7. Nomenclature

a	sonic speed
c_p	specific heat at constant pressure
f	frequency, Hz
h	specific sensible enthalpy
k	thermal conductivity
k_s	equivalent sand roughness height
p	static pressure
q	turbulence intensity, $\overline{(u'^2 + v'^2 + w'^2)}^{1/2}$
q_m	maximum value of q
R	inner radius of a cylindrical duct
Re_c	axial-flow Reynolds Number, $\bar{\rho}_c \bar{u}_c \delta / \bar{\mu}_c$
Re_s	injection Reynolds number, $\bar{\rho}_s \bar{v}_s \delta / \bar{\mu}_s$
Re_t	turbulence Reynolds number, $\bar{\rho} q \Lambda / \mu$
R_u	universal gas constant
t	time
T	static temperature
u_j	velocity vector (u,v,w)
x_j	coordinate vector (x,r,z)
x_o	axial distance at which computational initial conditions are specified
y	distance from surface distance from surface, $\delta - r$, (planar flow); or $R - r$, axisymmetric flow
ϕ	characteristic length scale
Λ	turbulence macro-length scale
μ	viscosity

ν	kinematic viscosity
ρ	density
σ	$= k/c_p$
σ_v	$= [\overline{v'v'}/\overline{v^2}]_s^{1/2}$
τ	turbulence shear stress
$\langle \rangle$	time mean of variable

Superscripts

—	average of variable over turbulent fluctuations
'	turbulent fluctuating value of variable
"	acoustic fluctuating value of variable

Subscripts

a	acoustic
c	duct centerline
e	value at edge of boundary layer
h	condition at port head end
m	max absolute value
s	condition at surface
,	differentiation

8. Publications

(of work supported by this grant)

During the period of performance, the following publication was issued based on work supported, in part, by the subject grant:

Beddini, R. A. and Roberts, T.A.; "Turbularization of an Acoustic Boundary-Layer on a Transpiring Surface"; Paper No. 86-1448, presented at the AIAA/ASME/SAE/ASEE 22nd Joint Propulsion Conf., Huntsville, AL, June 1986, (accepted for publication in the AIAA Journal).

9. Personnel

In addition to the Principal Investigator, Professor Robert A. Beddini, the following graduate students contributed technically to the overall research program effort and were supported principally or secondarily by AFOSR funds during the period of performance. Degrees being sought are given in parentheses.

Principal support was provided to:

Shyang-Lin Kuo	(Ph.D.)
Thomas G. Owano	(M.S.)
Ted A. Roberts	(M.S.)

Secondary (summer) support was provided to:

Claudia M. Bosch	(M.S.)
------------------	--------

10. Technical Interactions

During the period of performance, two principal technical interactions with industry representatives occurred and are presently noted.

- 1) At the AFOSR/RPL Rocket Propulsion research meeting in September, 1986, a technical discussion was held with Dr. Woodward Waeche of Atlantic Research Corp. Dr. Waeche requested the Principal Investigator to keep ARC apprised of the progress of the work, and to inform him should any immediate design guidelines for control of solid propellant instability be discovered.
- 2) At the AIAA Propulsion Conference (Huntsville) in July, 1986, a technical discussion was held with Dr. George B. Cox of Pratt and Whitney, Orlando. Dr. Cox expressed an interest in the work since P&W utilizes porous liners for passive stability control on several of its liquid engine combustion chamber designs. He requested to be kept informed of future work that included effects of combustion, heat transfer and active cooling of the chamber surface.

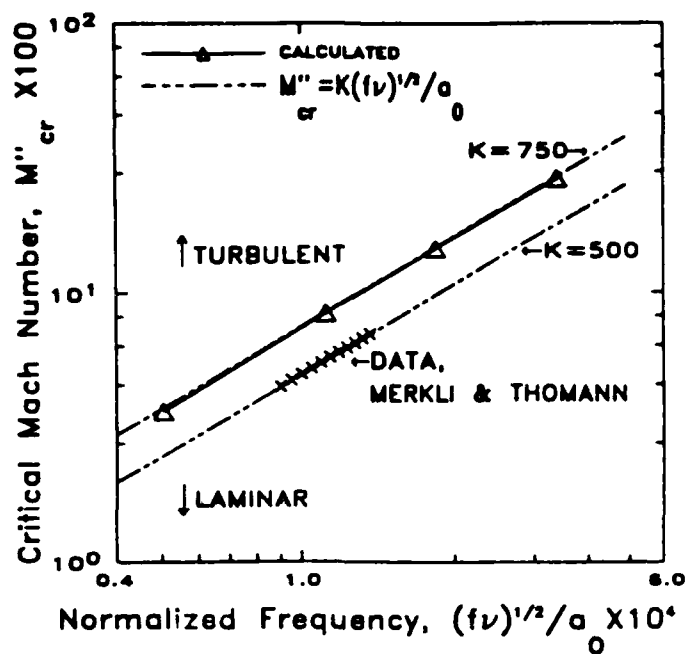


Figure 1. Transition to turbulence for simple acoustic motion.

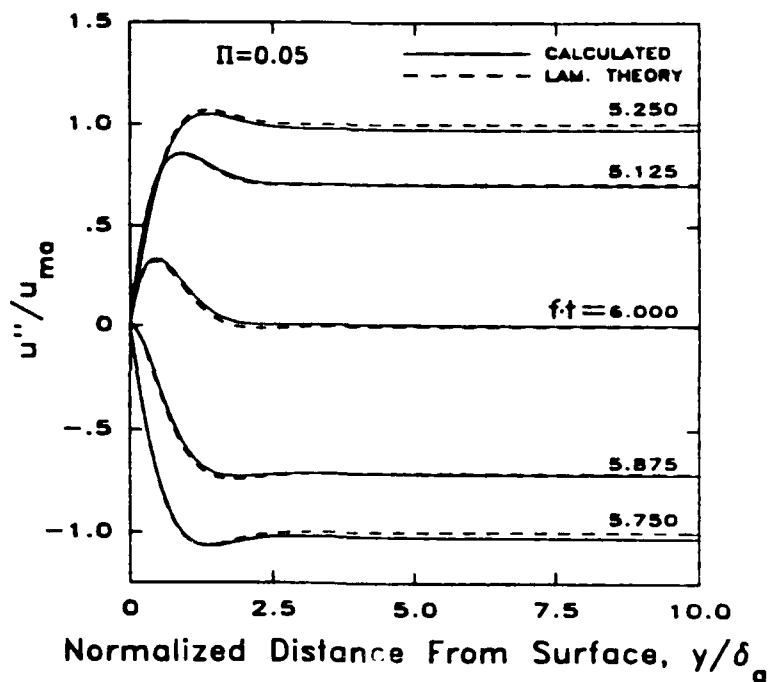


Figure 2. Laminar velocity profiles in the acoustic boundary layer without injection.

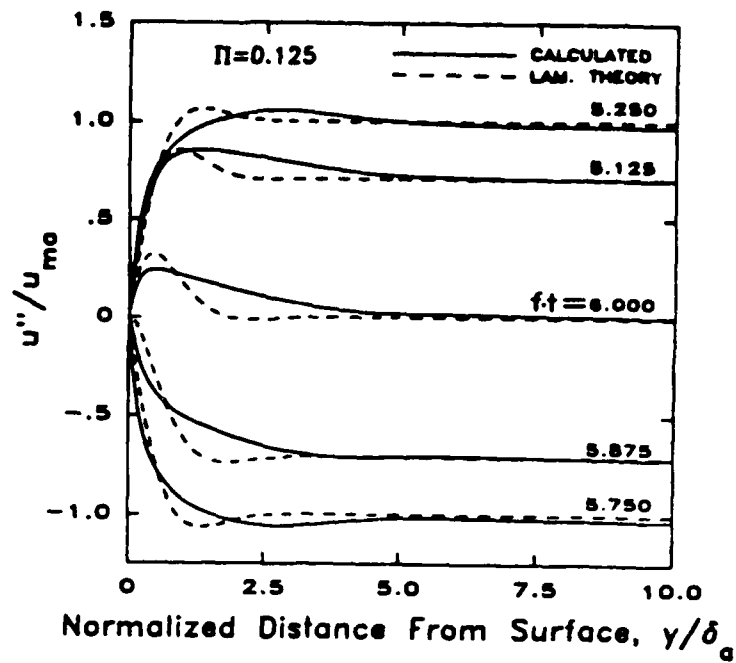


Figure 3. Turbulent velocity profiles in the acoustic boundary layer without injection.

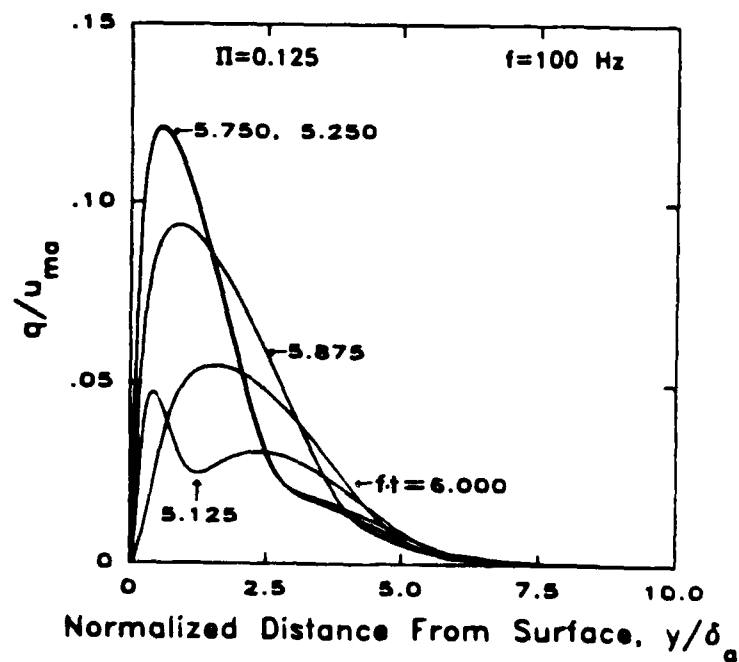


Figure 4. Turbulence intensity profiles in the acoustic boundary layer without injection.

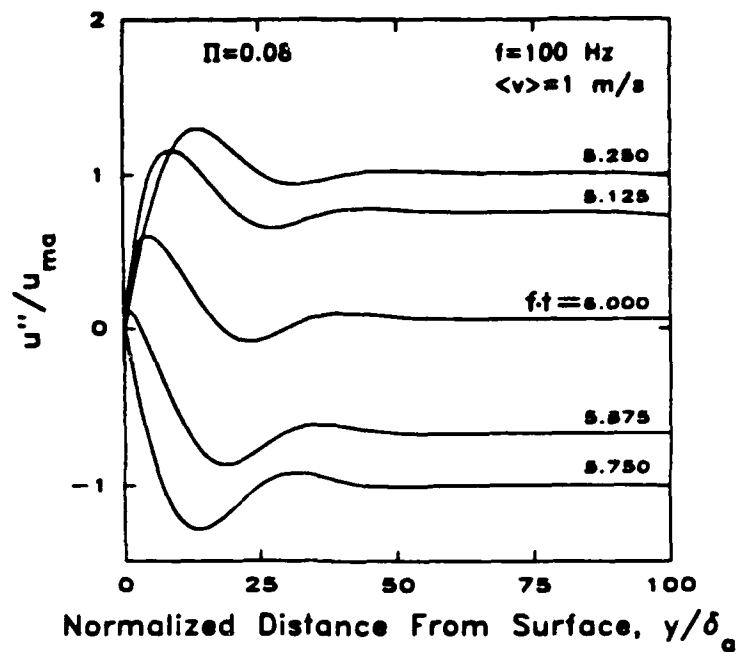


Figure 5. Turbulent velocity profiles in the acoustic boundary layer with injection.

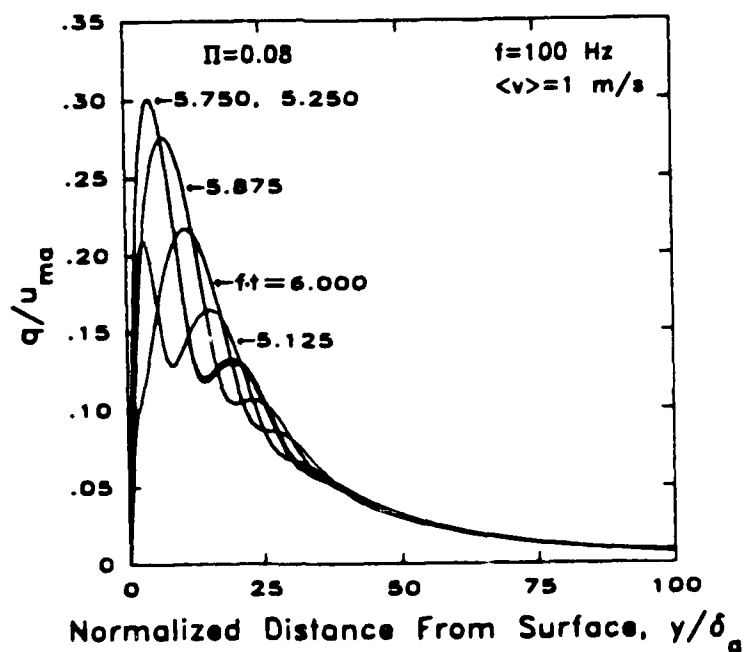


Figure 6. Turbulence intensity profiles in the acoustic boundary layer with injection.

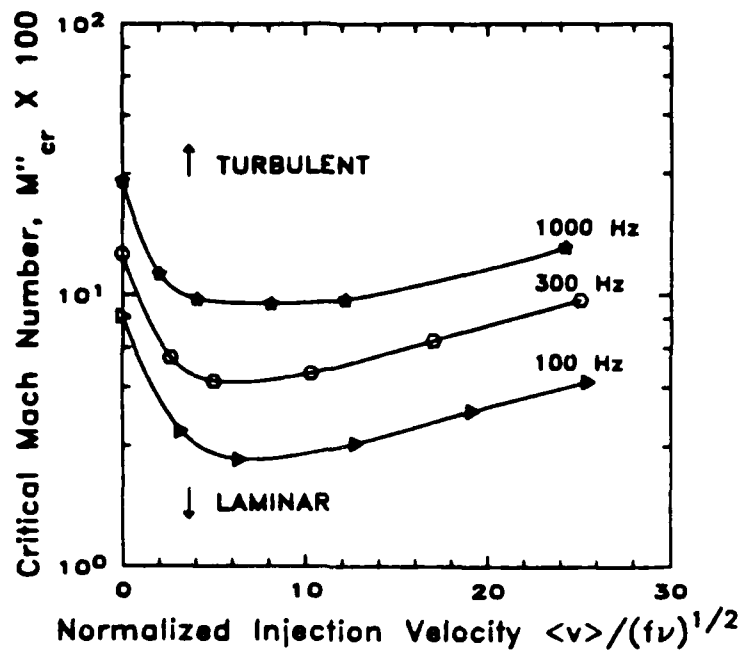


Figure 7. Effect of injection on the stability of the acoustic boundary layer.

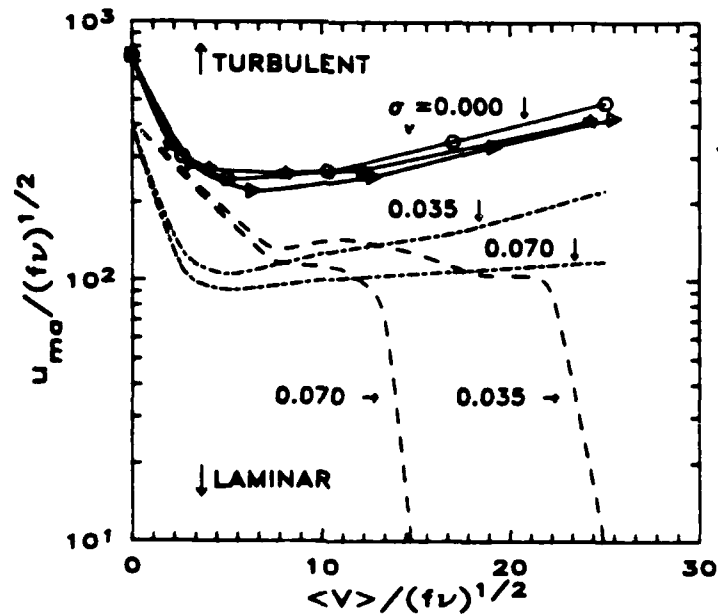


Figure 8. Effects of injection and injection disturbance level on the stability of the acoustic boundary layer.

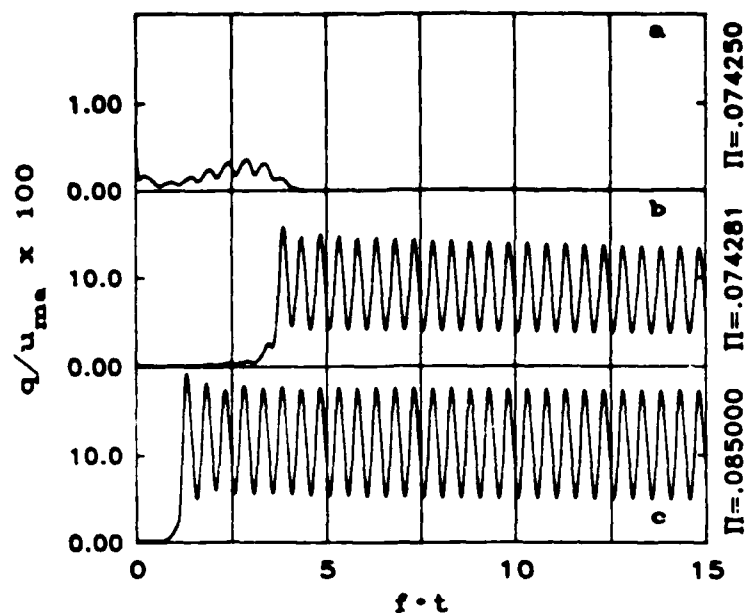


Figure 9 (a-c). Time variation of turbulence development for the injected acoustic boundary layer ($\sigma_v = 0$, $y = \delta_a$).

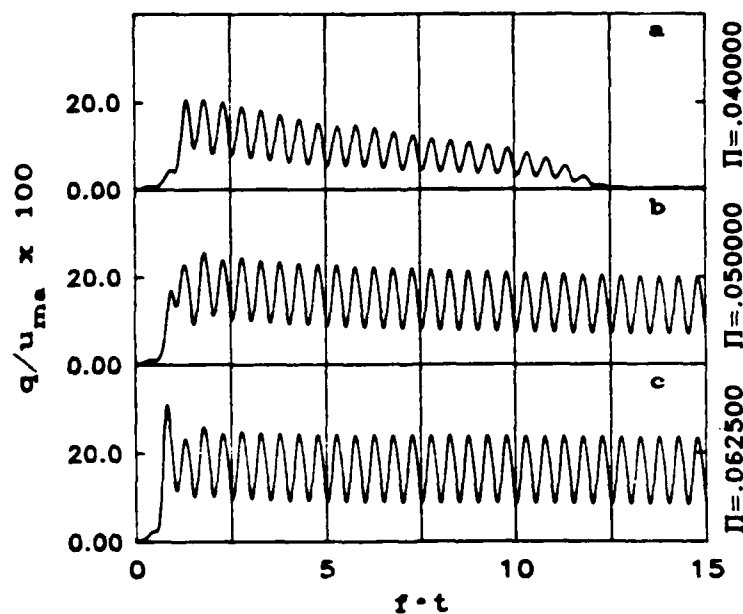


Figure 10 (a-c). Time variation of turbulence development for the injected acoustic boundary layer ($\sigma_v = 0.035$, $y = \delta_a$).

END

DATE

FILMED

JAN

1988